Journal of Materials, Processing and Design (2023)
Clausius Scientific Press, Canada

DOI: 10.23977/jmpd.2023.070108
ISSN 2516-0923 Vol. 7 Num. 1

Study on gas spark discharge plasma diagnosed by laser interferometric technology

Jie Huang[1,*], Zhe Liu[1], Jiangshan Chen[1], Haopeng Li[1]

[1]Nuclear Power Institute of China, Chengdu, China
[*]Corresponding author: 13311102482@163.com

Keywords: Air switch discharge plasma, laser interferometric technology, electron density, shock wave

Abstract: Laser interferometric technology is an important means for diagnosing plasmas due to its high temporal and spatial resolution. In this work, an air switch discharge plasma was diagnosed by a Mach-Zehnder laser interferometer with a wavelength of 532 nm. The air switch discharge plasma was generated between two needle-type Cu electrodes. Three dimensional electron density profiles of the air switch discharge plasma were deduced by numerical processing the interferograms containing plasma phase information obtained from experiments, revealing the formation and evolution processes of the arc channel of the air switch between the electrodes. At the start of the discharge, a large number of electrons were generated at the cathode, and then accelerated to the anode under the action of the electric field. During motion, neutral gas was ionized, and a cylindrical arc channel formed rapidly. A large pressure gradient was generated due to the dense plasma in the arc channel, so the dense plasma began to expand and push the surrounding air, forming a shock wave. The experimental results indicated that laser interferometric technology is an effective way to study air switch discharge plasmas.

1. Introduction

A gas spark switch is a key part of pulsed power technology. It is widely used in both national defense scientific research and industry [1-2]. An air switch is a kind of gas spark switch that uses air as an insulating medium, which plays an important role in pulsed power equipment. Investigations into the operating process of an air switch to improve its lifetime and reliability have very important significance.

The electron density distribution and evolution of air switch discharge plasma have a significant effect on the operating process of the air switch. A series of methods can be used to measure the electron density, such as the Langmuir probe method [3], emission spectroscopy method [4], Thomson scattering method [5], high-speed imaging method, and laser interference method [6]. However, the Langmuir probe method has a low accuracy and perturbs to the plasma. Although the Thomson scattering method has a high accuracy, the experimental setups are complex and expensive. The emission spectroscopy method requires the assumption of a balanced state model for the plasma, and it is difficult to determine the spectrum in this method. The high-speed imaging method cannot obtain quantitative plasma date. The laser interference method is the most important

means of diagnosing plasma because of its high temporal and spatial resolution. It neither disturbs the plasma nor requires the assumption of a balanced state model for the plasma, and the obtained plasma data is real-time and reliable. Based on the assumption of an axisymmetric plasma, 3D electron density profiles of the plasma can be obtained by an inverse Abel transformation.

Gas discharge is a transient and complicated physical process. Generally, the major physical processes of gas discharge contain two stages, plasma formation and plasma expansion. There is no clear threshold for the two stages. Once the plasma is produced, it will expand in the background gas, and shock waves will form because of a steep density gradient [7-8]. To comprehend the processes of plasma formation and plasma expansion in the background gas, many works have been carried out. Zhang H C *et al*. studied laser induced plasma in air using laser interferometry, and a 3D electron density profile was obtained. Hairlal *et al*. used the laser shadowgraph technique and a fluid simulation to study shock wave propagation, estimating the pressure and velocity of the shock front [9]. Yang Z F *et al*. studied laser induced copper plasmas in air using fast spectral imaging and two-color laser interferometry, and the density profiles of Cu atoms and electrons were obtained [10].

It is challenging to obtain the exact value of the plasma density especially the temporal and spatial evolution characteristics of the electron density. In this paper, a Mach-Zehnder (M-Z) laser interferometer with a laser wavelength of 532 nm was used to diagnose an air switch discharge plasma. Interferograms containing plasma phase information were obtained in the experiments. The three dimensional distribution of the electron density of the plasma under different time delays were obtained by numerical processing. The temporal and spatial evolution characteristics of the electron density were analyzed. Plasma shock waves were observed in these experiments. Meanwhile the reason for the production plasma shock waves was analyzed.

2. Theory and assumptions

As we know, plasma consists of electrons, ions and neutral atoms. Different types of particles have different contributions to the refractive index of plasma. For a plasma that consists of electrons, ions and the neutral atoms, the refractive index can be written as

$$n = 1 - \frac{e_0^2 \lambda^2 N_e}{8\pi^2 \varepsilon_0 m_e c^2} + \sum_{\kappa}\left(A_k + \frac{B_k}{\lambda^2}\right)\frac{N_k}{N_A} \tag{1}$$

where n is the refractive index of the plasma, λ is the wavelength of the probing laser beam, e_0 is the elementary charge, m_e is the electronic mass, ε_0 is the dielectric constant, c is the speed of light in vacuum, and N_A is Avogadro's constant. N_e is the number density of free electrons, and N_k is the number density of particles of type k. A_k and B_k denote the gas-specific constants for these particles, respectively. For equation (1), the first term is the contribution due to free electrons, and the second term is due to heavy particles (atoms and ions).

The influence of electrons on the refractive index is dominant for a low temperature plasma, especially when the electron density exceeds $2 \times 10^{19}\mathrm{cm}^{-3}$, the contribution to the refractive index from heavy particles can be neglected entirely. Thus, the electron density can be calculated from a refractive index distribution at a single probing wavelength:

$$N_e = \frac{8\pi^2 \varepsilon_0 m_e c^2}{e_0^2 \lambda^2}(n-1) \tag{2}$$

When the probing laser beam through the plasma and interferes with a reference laser beam in air, the recorded phase shift of the fringe, $\Delta\varphi$, is related to the refractive index of the plasma by

$$\Delta\varphi = \frac{2\pi}{\lambda}\int_{z_1}^{z_2}\{n - n_0\}dz \tag{3}$$

where $\Delta\varphi$ is the value of the phase shift of the probing laser beam passed through the plasma, n is the refractive index of the plasma, n_0 is the refractive index of air $(n_0 = 1.0003)$ and Z is the propagation path of the probing laser beam in the plasma.

Having digitized the interferograms and performed an inverse Abel transformation with the assumption of axial symmetry for the plasma. We can reconstruct a spatial distribution of the local values of the refractive index, and then a 3D spatial and temporal distribution of the electron density of the plasma can be obtained. For equation (3), the inverse Abel transformation can be written as

$$n(x,y,z) - n_0 = -\frac{\lambda}{\pi}\int_r^R \frac{d\Delta\varphi(x)/dx}{\sqrt{x^2-y^2}}dx \tag{4}$$

3. Experimental setup

All experiments were performed under atmospheric pressure. A schematic diagram of the experimental setup is shown in Figure 1. In these experiments, the output wavelength of the Q-switch Nd:YAG laser is 1064 nm and the full width at half maximum (FWHM) of the laser pulse is approximately 7 ns. The frequency of the output laser is doubled by a frequency doubling crystal (KDP) with a frequency doubling efficiency of 15% to provide a probing laser beam with a wavelength of 532 nm.

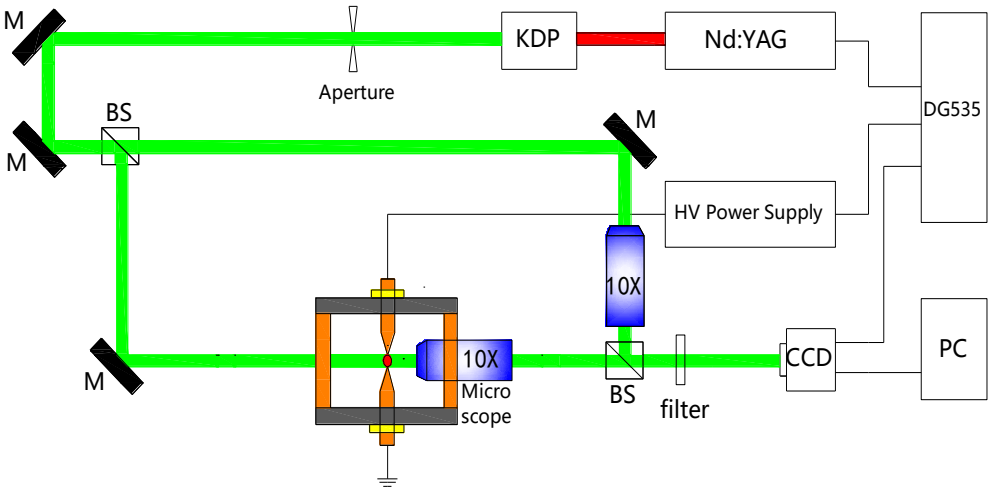

Figure 1: The experimental setup for laser interferometry to diagnose the air switch discharge plasma: KDP=potassium dihydrogen phosphate, M=mirror, BS=beam splitter, CCD=CCD camera, PC=personal computer, DG645=digital delay pulse generator, HV power supply= high voltage pulsed power supply

The probing laser beam with a wavelength of 532 nm passes through an optical path delay system consisting of two mirrors and then separated into two beams by a Mach-Zehnder interferometer. Plasma is produced in one arm of the Mach-Zehnder interferometer. The laser beam that passes through the plasma is called the probe beam and the other beam that does not pass through the plasma is called the reference beam. Two laser beams (the probe beam and the reference beam) merge together at the beam splitter and produce an interferogram on the charge coupled device (CCD) camera. The CCD camera is connected to a personal computer that is used to display and store the interferograms in real time. To eliminate the effects of plasma luminescence and other stray light and improve the contrast of the interferograms, a bandpass filter ($\lambda = 532$ nm, FWHM $=$ 1 nm) is used in front of the CCD camera. Two microscopes (magnification of 10X) are installed in

each arm of the Mach-Zehnder interferometer to improve the spatial resolution of the interferometer. Therefore, a spatial resolution of approximately 5 μm can achieved.The temporal resolution of the interferometer is determined by the pulse duration of the probing laser beam and is approximately 7 ns. In these experiments, a digital delay pulse generator (DG535) is used to control the timing of the laser, the high voltage power supply and the CCD camera. Thus, the interferograms containing plasma phase information for different time delays can be obtained.

In our experiments, the air switch was simplified as a two electrodes tip discharge structure, which schematic diagram is shown in Figure 2. Plasma was generated between two needle-type copper electrodes with a gap between the electrodes of 2 mm. The arc discharge was ignited in self-breakdown mode. The output high voltage of the high-voltage pulse power supply is 10 kV, the discharge current amplitude is 50 A and the discharge duration is 3 microseconds. The stability of the needle-type electrode discharge ensures good experimental repeatability.

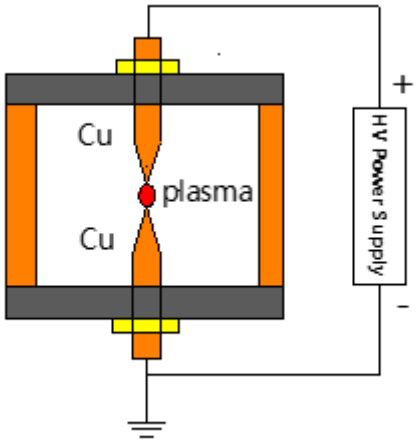

Figure 2: Simplified discharge device schematic diagram. The simplified air switch is works in self-breakdown mode. The gap between the electrodes is 2 mm. The output voltage of the HV Power Supply is 10 kV, the current amplitude is 50 A and the discharge duration is 3 microseconds.

4. Results and Discussions

4.1 Interferograms

Although the experimental setup can obtain only one interferogram in a single discharge, the discharge of the high voltage pulse power is stable, so the time jitter of the high voltage pulse power is very small. The needle-type electrode discharge structure ensures discharge at the tip of the electrode. Therefore, the good reproducibility of the experiment can be ensured. Thus, interferograms for different delay times can be recorded to study the temporal and spatial evolution of the air switch discharge plasma. Typical interferograms as a function of the time delay are presented in Figure 3. Interferogram (a) was obtained when electrical break down in electrode gap occurred and plasma was generated. For the recording and analysis, the moment at which interferogram (a) was captured was defined as time zero. In interferogram (a) the interference fringes bend and shift, especially near the cathode, which indicates that a large plasma was produced near the cathode at this moment. Interferogram (b) was obtained at t=10 ns. An arc channel completely formed, and a typical columnar arc channel can be observed in interferogram (b). Interferogram (c) was obtained at t=75 ns. From interferogram(c), we see that the plasma spread into the surrounding air, and the shock wave began to gradually forme due to the spread of the plasma compressing the air. Interferogram (d) was obtained at t=130 ns, at the moment the

plasma spread completely into the surrounding air. The shock wave grew in size due to the push of the plasma. Interferogram (e) and interferogram (f) were obtained at t=240 ns, and t=420 ns, respectively.

It can be seen from Figure 3 that the interferograms have high contrast and low noise. In these interferograms, it is clear that the interference fringes bend and shift. These interferograms show the spatial and temporal evolution of the air switch discharge plasma, which can be used to measure the plasma electron density, plasma volume, and expansion velocity.

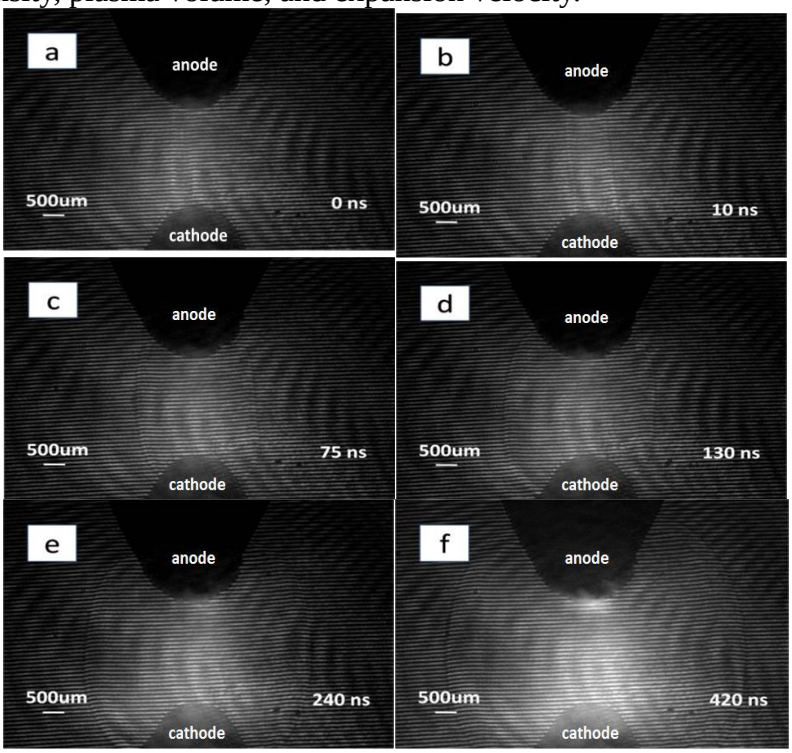

Figure 3: Interferograms of air switch discharge plasma under different delay times. Interferogram (a) was obtained at the beginning of the arc channel formation. The moment at which interferogram (a) was captured was defined as time zero. Interferogram (b) was obtained at t=10 ns, interferogram (c) was obtained at t=75 ns, interferogram (d) was obtained at t=130 ns, interferogram (e) was obtained at t=240 ns, and interferogram (f) was obtained at t=420 ns.

4.2 Phase shift extraction from interferograms

The phase shift $\Delta\varphi$ is the most crucial parameter for calculating the electron density of plasma. First, we digitized the interferograms, and the phase shift of the interferograms was extracted by 2D fast Fourier transform (FFT) analysis. Because the resulting phase from the 2D FFT analysis is wrapped into the interval $[-\pi, +\pi]$, to obtain a continuous phase, a phase unwrapping algorithm must be performed. An air switch discharge plasma has a dense density and a steep pressure gradient at atmosphere pressure always drives a shock wave, which can induce a phase discontinuity. In this paper, the phase unwrapping algorithm using graph cuts is applied to obtain a continuous phase distribution. Figure 4 shows the continuous phase shift distributions from the interferograms of Figure 3.

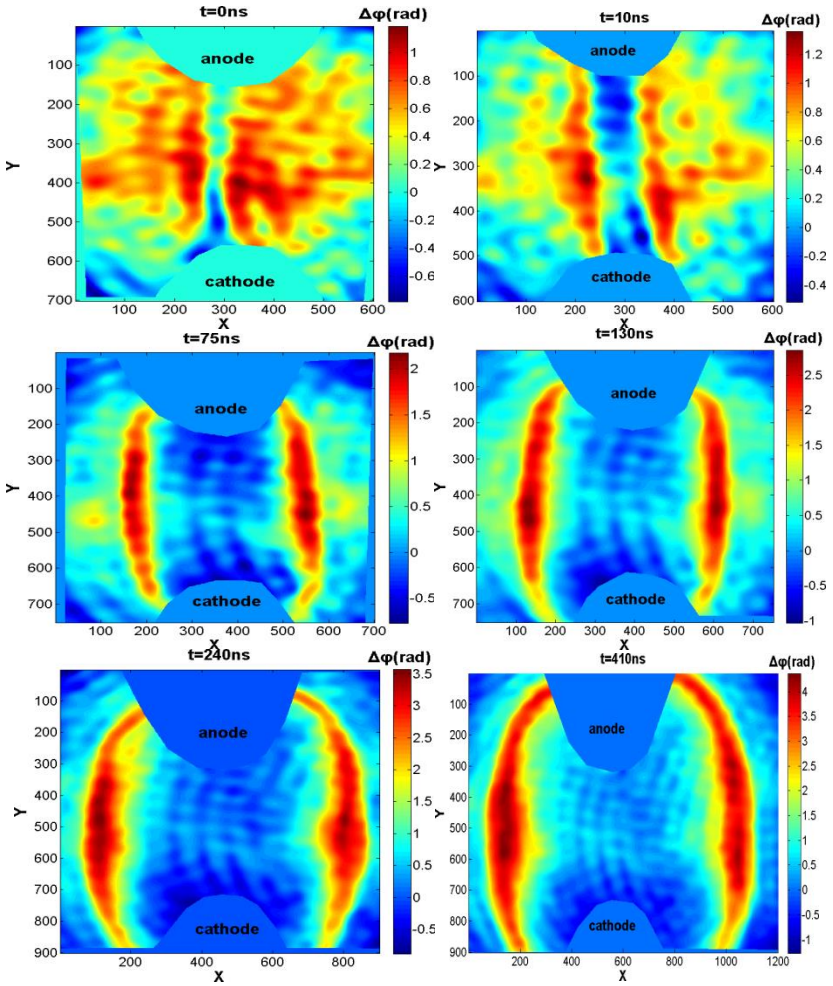

Figure 4: Phase shift extracted from the interferograms of Figure 3 as false color images. The values of the x and y axes represents the pixel points. The phase shift $\Delta\varphi$ is expressed in radians.

As indicated in Figure 4, the phase shifts were extracted from the interferograms of Figure 3 and represented as false color images. According to equation (1), the refractive index of the plasma mainly consists of two parts: free electrons and heavy particles (neutral atoms and ions). The phase shifts contributed by heavy particles and electrons are opposite in sign. As shown in Figure4, some areas have a darker color (positive phase shift) around the electrodes and an obvious ring structure; this is the dense compressed air layer containing many neutral atoms that forms due to the spreading of the plasma. However, there are many free electrons between the electrodes, leading to a negative phase shift in the region of the plasma. The dense compressed air layer exhibits a clear plasma boundary, so we can observe the plasma shape after diffusion is complete.

4.3 Electron density distribution

From Figure 4, we can see that the phase shift of the plasma is symmetric. Therefore, an inverse Abel transformation was applied to calculate the refractive index of the plasma. Then, the temporal and spatial evolution of the electron density distribution was obtained as presented in Figure 5.

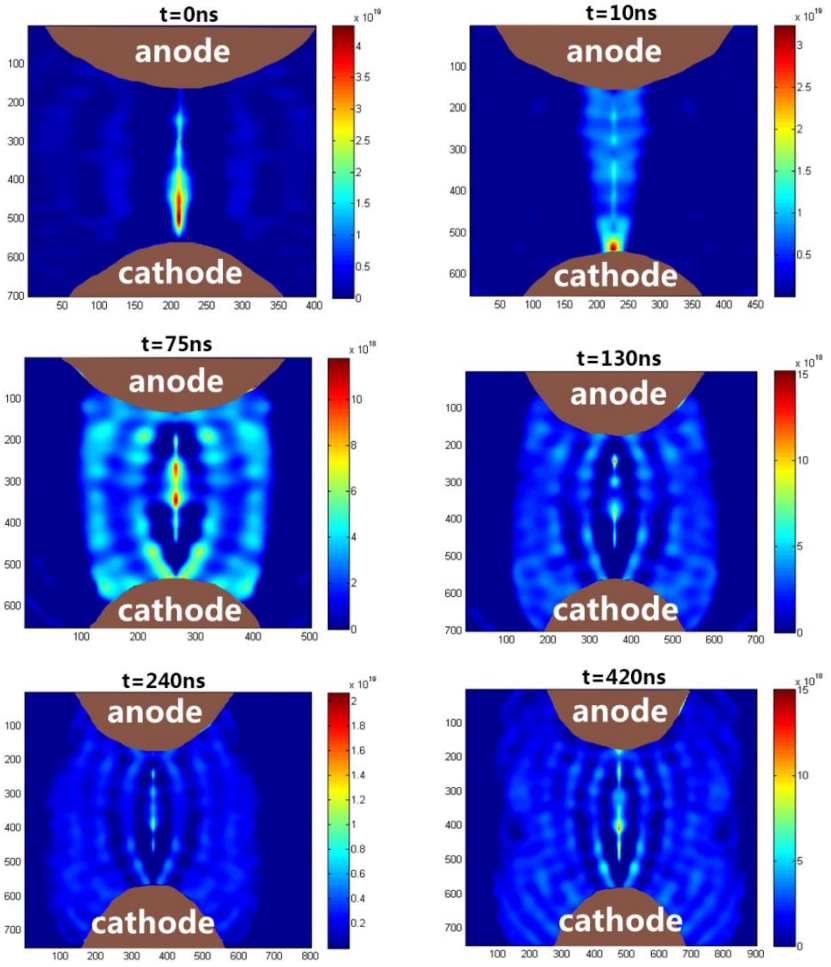

Figure 5: Temporal and spatial evolution of the electron density distribution of the air switch discharge plasma under different delay times as false color images. The delay times are t=0 ns, t=10 ns, t=75 ns, t=130 ns, t=240 ns and t=420 ns.

Figure 5 shows the temporal and spatial evolution of the electron density distribution of the air switch discharge plasma under different delay times as false color images. Figure 5 shows that at the beginning of the arc channel formation (t=0 ns), a large number of electrons accumulated around the cathode with an electron density greater than 4.3×10^{19} cm^{-3}. This value is very high. It is difficult to calculate the precise electron density because of the steep plasma density gradients. Due to the action of the electric field, a large number of electrons moved toward the anode and constituted a complete arc channel in a very short time. At t = 10 ns, as shown in Figure 5, a complete arc channel formed with a cylindrical arc channel structure, and an average electron density in the arc channel of 5.4×10^{18} cm^{-3} can be derived. Subsequently, the plasma began to expand into the surrounding air with a large pressure gradient. In the expanding process, the average electron density of the plasma gradually decreased, the plasma radius gradually increased and the diffusion velocity of the plasma gradually decreased.

Through numerical processing of the plasma electron density distributions, the 3D patterns calculated as shown in Figure 6. Figure 6 clearly shows the temporal and spatial evolution of the electron density distribution of the air switch discharge plasma.

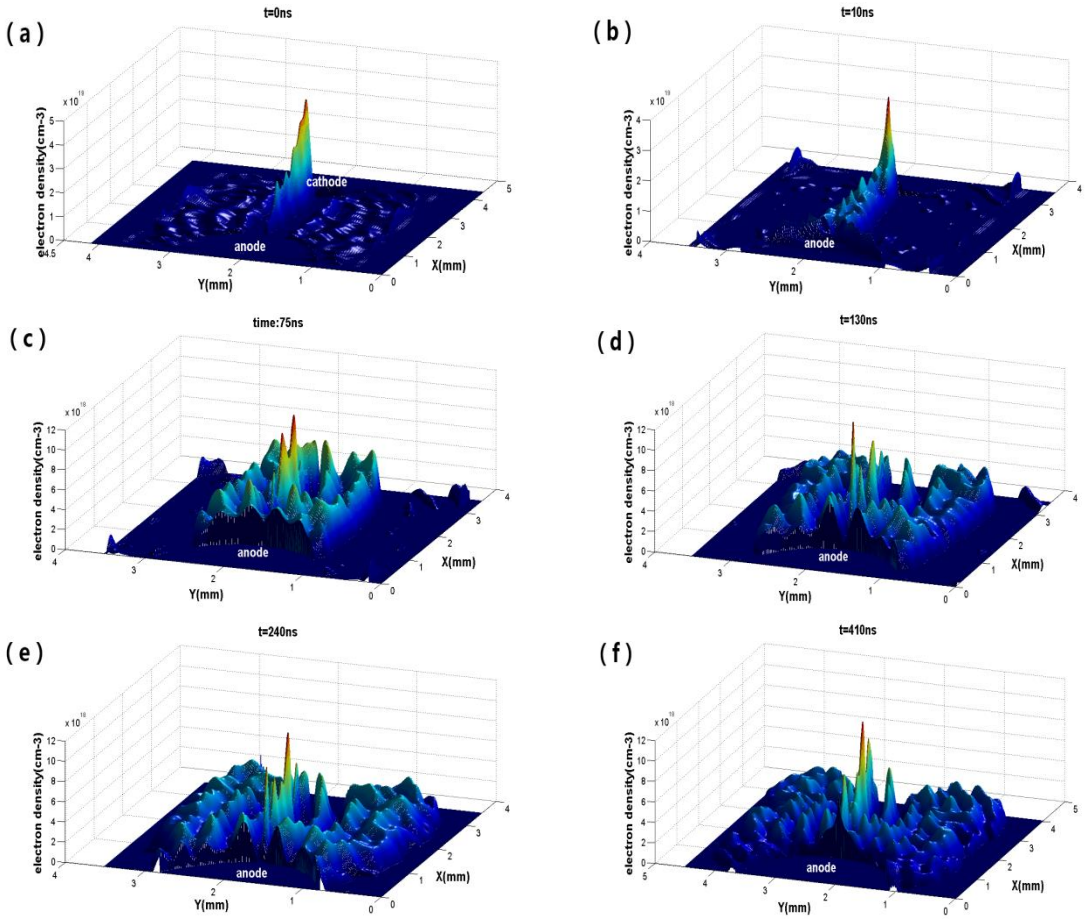

Figure 6. The plasma electron density 3D distributions of air switch. The delay time is (a), (b), (c), (d), (e), (f) t=0ns, t=10ns, t=75ns, t=130ns, t=240ns, t=420ns, respectively.

The changing average electron density, radius of the plasma and plasma diffusion velocity with time are shown in Figure 7. There are a large number of electrons between the electrodes when the arc channel was formed. Because of the avalanche ionization mechanism, a dense plasma is produced in a very short period of time. The dense plasma has an electron density greater than 4.3×10^{19} cm^{-3}, especially in the middle of the arc channel, which has a very high electron density. Therefore, the dense plasma has a very steep density gradient. Driven by the density gradient, the plasma will expand into the air. At the beginning when the plasma expands into the air, the plasma has a high average electron density. The diffusion process rapidly reduces the average electron density, and the radius of plasma increases rapidly. After approximately 100 ns, the average electron density of plasma tends is constant about $Ne = 2 \times 10^{18}$ cm^{-3}. Then, the average electron density decreases with time slowly due to continued expansion, as shown in Figure 7(a). There are two main reasons for the stabilized average electron density. First, high-speed electrons can ionize some of the neutral particles, and the secondary electrons compensate for the reduction in electron density caused by diffusion. Second, compared with the ion velocity, the electron velocity is much faster. Thus, the internal electric field of the plasma can be rapidly enhanced, which suppresses the continued diffusion of high-speed electrons and forces return of the electrons.

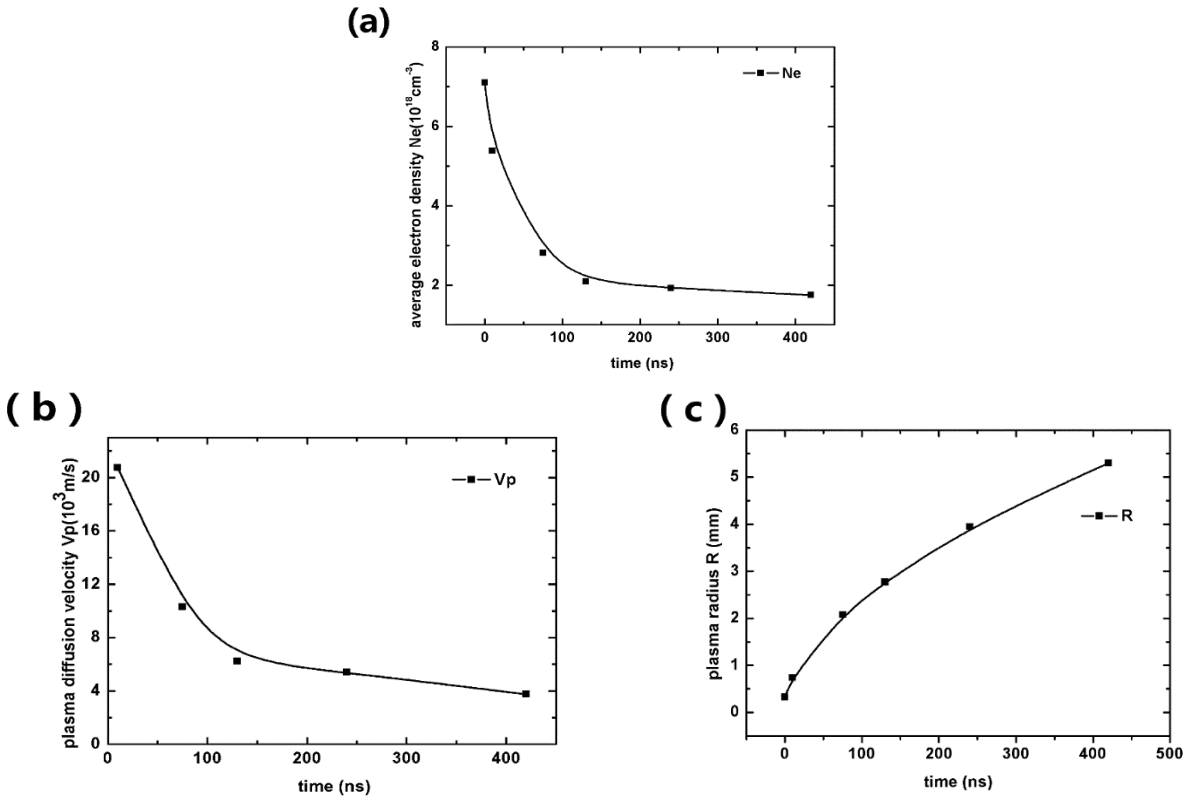

Figure 7: The average electron density (a), plasma diffusion velocity (b) and radius of the plasma (c) as a function of time.

The plasma diffusion velocity V_p as a function of time is shown in Figure 7(b). At the beginning of the plasma generation, the electron density gradient of plasma is very high, and the temperature of the plasma rapidly increases due to intense collisions between particles. Thus, the plasma rapidly expanded into air, and the initial diffusion velocity reached $V_p = 2.1 \times 10^4$ m/s. However, the temperature and density gradient of the plasma rapidly decreased as the plasma expanded. Therefore, the plasma diffusion velocity V_p rapidly reduced but was still above 1×10^3 m/s. Obviously the plasma diffusion velocity V_p is greater than the speed of sound, so the expansion of the plasma into air will form a significant shock wave, as was observed in the interferograms. However, the radius of the plasma continues to increase because the plasma expands, as shown in Figure 7(c). In the early phase of the plasma expansion, the radius of the plasma increases faster than after the expansion. The radius of plasma is approximately $R = 5.4$ mm after 420 ns. Similarly, the reason is that the plasma has a higher temperature and density gradient in the early stages of expansion.

5. Conclusions

In this paper, an air switch discharge plasma was diagnosed by a Mach-Zehnder laser interferometer with a wavelength of 532 nm. High quality interferograms were obtained. First, the phase shift was extracted by FFT analysis. Second, under the assumption of the plasma having cylindrical symmetry, an inverse Abel transformation was applied to obtain the refractive index of the plasma. Finally, 2D and 3D spatial and temporal distributions of the electron density were calculated.

The temporal and spatial evolution of the plasma was analyzed. In the initial stage of arc channel

formation, the electron density was as high as $4.3 \times 10^{19}\ \mathrm{cm}^{-3}$. Subsequently, the plasma rapidly diffused and the plasma radius increased rapidly under the high temperature and high density gradient. Then, the electron density decreased rapidly to $2 \times 10^{18}\ \mathrm{cm}^{-3}$ after approximately 100 ns as the temperature and density gradient rapidly reduced. By calculating the plasma diffusion velocity, it was found that the plasma diffusion velocity reaches $2.1 \times 10^{4}\ \mathrm{m/s}$ at the beginning of the diffusion process, and then decreases rapidly but still maintains a value above $1 \times 10^{3}\ \mathrm{m/s}$. The calculated result shows that the air switch discharge plasma diffuses a supersonic velocity, driving the air to form a compressed air layer. The high-speed propagation of the compressed air layer has the characteristics of a shock wave.

Research on the reliability of air switches, is necessary for accurate diagnosis of air switch discharge plasmas, and laser interferometric techniques provide a reliable method for accurately diagnosing such plasma. This work can provide a theoretical basis and experimental data for the operating process of an air switch.

References

[1] Cheng X B, Liu J L, Qian B L. 2010, IEEE Trans. on Plasma Science, 38(3):516-523
[2] Li N, Liu G, Guo L F, et al. 2011, Chin.Soc .for Elec. Eng., 31(6):109-115
[3] Chen L, Jin D Z, Tan X H. 2010, Vacuum. 85:813-816
[4] Yang L, Tan X H, Wan X, et al. 2014, Appl. Phys, 115, 163106
[5] Nedanovska E, Nersisyan G, Morgan T, et al, 2011, Applied Physics Letters, 99(26): 261504
[6] Zhang H C, Lu J, Ni X W, 2009, Chin. Phys. Soc., Vol. 58, No. 6, Jun
[7] S. S. Harilal, B. E. Brumfield, and M. C. Phillips, 2015, Phys. Plasmas 22, 063301
[8] J. Grun, J. Stamper, C. Manka, J. Resnick, 1991, Phys. Rev. Lett. 66, 2738
[9] S. S. Harilal, G. V. Miloshevsky, P. K. Diwakar, 2012, Phys. Plasmas 19, 083504
[10] Yang Z F, Wu J, Wei W F. et al. 2016, physics of plasma, 23, 083523